Monomeric Spin Density Distribution in the Primary Donor of Photosystem I as Determined by Electron Magnetic Resonance: Functional and Thermodynamic Implications

Michelle Mac,[†,§] Neil R. Bowlby,[‡] Gerald T. Babcock,[†] and John McCracken*[,†]

Contribution from the Departments of Chemistry and Biochemistry, Michigan State University, East Lansing, Michigan 48824

Received July 27, 1998. Revised Manuscript Received October 19, 1998

Abstract: The primary electron donor (P_{700}) in Photosystem I (PSI) has been shown to be a dimeric chlorophyll a species. Electron magnetic resonance studies of the cation radical have clearly established that the unpaired electron is delocalized asymmetrically over this dimer; however, the extent to which this asymmetry exists remains ambiguous. Comprehensive electron nuclear double resonance (ENDOR) and electron spin−echo envelope modulation (ESEEM) experiments combined with isotopic substitution and numerical simulations have been used to determine the electronic structure of P_{700}^+. This approach utilizes the strengths of each spectroscopy to elucidate the electron nuclear hyperfine and nuclear quadrupole coupling constants for the nitrogen nuclei in P_{700}^+. These assignments are then confirmed by performing numerical simulations of the ESEEM data. Further confirmation of these values is obtained by performing the spin−echo experiments at multiple microwave frequencies. The same set of hyperfine and quadrupole coupling constants is used to simulate all of the ESEEM data for P_{700}^+ containing either natural abundance ^{14}N or isotopically enriched with ^{15}N. These simulations indicate that the unpaired spin is localized over only one of the chlorophylls that make up the special pair. The ramifications of this monomeric spin density on the function and thermodynamics of electron transfer in PSI are discussed.

Introduction

Oxygenic photosynthesis in higher plants and cyanobacteria requires the interplay of two pigment−protein reaction centers, Photosystem I and Photosystem II (PSI and PSII, respectively). PSII is the site of water oxidation and oxygen evolution,[1−3] while PSI mediates the production of the reduced NADPH that is used by the plant in the dark reactions of the Calvin cycle.[4−7] In each system, the primary photochemistry proceeds through the generation of a specialized chlorophyll a (chl a) cation radical species (P_{700}^+ in PSI and P_{680}^+ in PSII). The concomitant generation of a transmembrane proton gradient drives ATP synthesis. Elucidation of the geometric and electronic structures of the primary donor cation radicals can yield important information regarding the electronic coupling within these molecules, the energetics of the system, and the early electron-transfer events and, moreover, help to explain the lack of significant charge recombination in a system that operates with a near unity quantum yield.

Significant progress[8−10] has been made in solving the crystal structure of PSI, with the recent 4.5 Å structure suggesting that P_{700}, in its ground state, is most likely a dimer of chl a,[8] thus confirming early resonance Raman results.[11] These data, while providing a clearer view of the geometric structure of the neutral species, do not provide information regarding the electronic structure of the cation radical.

EPR spectroscopy is an invaluable tool for the study of these structures since determination of the electron nuclear hyperfine coupling constants provides a direct measurement of the unpaired electron spin density distribution and, therefore, the highest occupied molecular orbital. The EPR signal from P_{700}^+ precludes determination of this information, however, since it consists only of a single line, inhomogeneously broadened by the presence of multiple hyperfine interactions.[12,13] To resolve these couplings, advanced EPR techniques can be used. Electron nuclear double resonance (ENDOR) and electron spin−echo envelope modulation (ESEEM) spectroscopies, in particular, are valuable in determining hyperfine couplings for inhomoge-

[†] Department of Chemistry.

[‡] Department of Biochemistry.

[§] Current address: Department of Natural Science, Lakeland College, P.O. Box 359 Sheboygan, WI 53082.

(1) Tommos, C.; Babcock, G. T. *Acc. Chem. Res.* **1998**, *31*, 18−25.

(2) Diner, B. A.; Babcock, G. T. Structure, Dynamics and Energy Conversion Efficiency in Photosystem II. In *Oxygenic Photosynthesis: The Light Reactions*; Ort, D., Yocum, C. F., Eds.; Kluwer Academic Publishers: Dordrecht, The Netherlands, 1996; pp 213−247.

(3) Britt, R. D. Oxygen evolution. In *Oxygenic Photosynthesis: The Light Reactions*; Ort, D., Yocum, C. F., Eds.; Kluwer Academic Publishers: Dordrecht, The Netherlands, 1996; pp 137−164.

(4) Fromme, P. *Curr. Opin. Struct. Biol.* **1996**, *6*, 473−484.

(5) Brettl, K. *Biochim. Biophys. Acta* **1997**, *1318*, 322−373.

(6) Malkin, R. In *Oxygenic Photosynthesis: The Light Reactions*; Ort, D., Yocum, C. F., Eds.; Kluwer Academic Publishers: Dordrecht, The Netherlands, 1996.

(7) Golbeck, J. *Annu. Rev. Plant Physiol. Plant Mol. Biol.* **1992**, *43*, 293.

(8) Fromme, P.; Witt, H. T.; Schubert, W.-D.; Klukas, O.; Saenger, W.; Krauss, N. *Biochim. Biophys. Acta* **1996**, *1275*, 76−83.

(9) Krauss, N.; Schubert, W. D.; Klukas, O. *Nat. Struct. Biol.* **1996**, *3*, 965−973.

(10) Schubert, W. D.; Klukas, O.; Krauss, N.; Saenger, W.; Fromme, P.; Witt, H. T. *J. Mol. Biol.* **1997**, *272*, 741−769.

(11) Moenne-Loccoz, P.; Robert, B.; Ikegami, I.; Lutz, M. *Biochemistry* **1990**, *29*, 4740−4746.

(12) Commoner, B.; Heise, J. J.; Townsend, J. *Proc. Natl. Acad. Sci. U.S.A.* **1956**, *42*, 710−718.

(13) Norris, J. R.; Uphaus, R. A.; Crespi, H. L.; Katz, J. J. *Proc. Natl. Acad. Sci. U.S.A.* **1971**, *68*, 625−628.

10.1021/ja982662i CCC: $15.00 © 1998 American Chemical Society
Published on Web 12/03/1998

neously broadened lines. In P_{700}^+, contributions from multiple interacting nuclei increase the complexity of both the ENDOR and ESEEM spectra, making specific assignments difficult. This is exemplified by recent independent ENDOR (^{1}H and ^{15}N),[14−16] ESEEM,[15,17,18] and HYSCORE (hyperfine sublevel correlation spectroscopy, or two-dimensional ESEEM)[19,20] experiments on frozen solutions and single crystals of PSI. These studies have clearly established that P_{700}^+ is composed of a dimer of chl a with an asymmetrical spin density distribution similar to that found in bacteria,[21] although they have not been conclusive in determining either the nitrogen hyperfine or quadrupole coupling constants for the cation radical. Thus, the degree to which this asymmetry exists remains ambiguous.

To circumvent the complexity induced by the electron−nuclear hyperfine interactions of up to 10 nitrogen nuclei—8 from the two chlorophylls of P_{700} and possible 2 from the histidine ligands—a more comprehensive approach must be undertaken. The application of both ESEEM and ENDOR, in conjunction with isotopic enrichment and numerical simulations of multifrequency ESEEM data provides the constraints necessary to assign, without ambiguity, the resonances observed in the ENDOR and ESEEM experiments. The utility of this approach has been demonstrated previously by this laboratory in identifying the axial histidine ligand to P_{700}^+.[22]

Briefly, we use multifrequency ESEEM on PSI containing natural abundance ^{14}N to elucidate all of the nitrogen nuclear quadrupole coupling parameters. By performing the experiment at multiple microwave frequencies, we are able to determine the exact cancellation conditions for the various nitrogen nuclei contributing to the spectrum. Moreover, since the exact cancellation condition occurs when the hyperfine and nuclear Zeeman fields cancel, this information provides constraints on the magnitude of the isotropic contribution to the nitrogen hyperfine coupling. The anisotropic contribution to the hyperfine coupling can be determined from ^{15}N ENDOR experiments on PSI uniformly labeled with ^{15}N. In these experiments, the perpendicular components of the nitrogen hyperfine tensors can be resolved and, in conjunction with multifrequency ^{15}N ESEEM, assigned. All of the coupling constants determined from the experimental data are confirmed by performing numerical simulations of the ESEEM data taken at multiple microwave frequencies on samples containing either ^{14}N or ^{15}N. Ambiguity in these assignments can be removed by using the same set of parameters to simulate all of the experimental ESEEM data. This comprehensive approach to solving the electronic structure of P_{700}^+ is used here to determine that the unpaired electron spin in P_{700}^+ is completely localized on one of the chlorophylls in the dimer pair.

Materials and Methods

Growth of Cells. Cells of *Synechocystis PCC* 6803 were grown under photoautotrophic conditions, with aeration, in BG-11.[23] To label cells uniformly with ^{15}N, KNO_3 in the growth medium was replaced entirely by $K^{15}NO_3$ (purity >98%, Cambridge Isotope Laboratories, Andover, MA). When cell growth had reached the late log phase (o.d. 600 > 1.2), the cells were harvested by continuous-flow centrifugation at 4° C, washed twice, and resuspended in BG-11. Glycerol was added to the cell suspension to 15% (v/v), the suspensions were mixed thoroughly and stored at −70 °C.

Preparation of Photosystem I Particles. Thylakoid membrane preparation and purification of the photosystems was performed essentially as described in Noren et al.[24] Frozen cells, equivalent to about 20−25 of mg chlorophyll, were thawed quickly and diluted with break buffer (0.8 M sucrose, 50 mM MES, pH 6.0) into a 250 mL centrifuge bottle. Cells were pelleted by centrifugation at 10 000*g* for 10 min, resuspended in a small volume of break buffer and transferred to a bead-beater chamber. Solubilization of thylakoid membranes and anion-exchange chromatography were carried out as described[24] except that fractions from the Q-Sepharose Fast Flow column which were enriched in PSI (λ_{max} > 679 nm) were pooled and precipitated by the addition of an equal volume of 30% (w/v) PEG-8000 in 50 mM MES, pH 6.0. After mixing, the preparation was incubated overnight at 4 °C, and the resulting precipitate was recovered by centrifugation at 20 000*g* for 10 min. The pellet was redissolved in Mono-Q start buffer (25% (v/v) glycerol, 0.05% lauryl maltoside, 50 mM MES, pH 6.5, 20 mM $CaCl_2$, 15 mM NaCl), and the solution was chromatographed on the Mono-Q column. Fractions enriched in PSI were pooled, and an equal volume of 30% PEG-8000 was added followed by centrifugation at 40 000*g* for 30 min. The supernatant was removed completely, and the pellet was resuspended in 50 mM HEPES pH 7.5, 15 mM NaCl, 0.05% dodecyl maltoside to a final concentration of >3 mg of chlorophyll/mL. The sample was then transferred to a 4 mm o.d. quartz EPR tube and stored in liquid nitrogen until further use. P_{700}^+ was generated by illumination at 273 K for 30 s. The radical was trapped by freezing immediately to 77 K. The radical's presence, in both natural abundance ^{14}N and isotopically enriched ^{15}N samples, was confirmed by CW-EPR. The isotope composition of the chlorophyll a extracted from ^{15}N-labeled PSI was determined by using FAB-MS, which was performed at the Michigan State University Mass Spectrometry Facility.

Continuous Wave EPR. The CW-EPR data were obtained (10 K) at X-band on a Bruker ER200D EPR spectrometer outfitted with a Bruker TE102 EPR cavity and an Oxford ESR-900 continuous flow cryostat. Microwave frequency was determined by using an EIP Microwave Model 25B frequency counter and the static magnetic field strength was measured with a Bruker ER035N NMR gaussmeter.

ENDOR Spectroscopy and Data Analysis. The ENDOR data were obtained at X-band on a Bruker ESP300e spectrometer with a Bruker ESP360 DS ENDOR accessory and home-built removable coils.[25] All ENDOR data were collected at a field position corresponding to the center of the EPR absorption line. Constant temperature in the cavity was maintained with an Oxford ESR900 continuous flow cryostat. Microwave frequency and static magnetic field strength were calibrated as mentioned above.

The peaks attributed to ^{15}N ($I = {}^1/_2$) electron nuclear hyperfine coupling are expected to be split symmetrically about the nuclear Larmor frequency for ^{15}N ($\nu_{15N} = 1.45$ MHz at 350.0 mT). In solution ENDOR, the position of these peaks is indicative of the strength of the isotropic hyperfine coupling according to the relationship[26]

$$\nu_+ = \nu_n \pm A_{iso}/2$$

(14) Lubitz, W. In *Chlorophylls*; Scheer, H., Ed.; CRC: Boca Raton, FL, 1991; p 903.
(15) Kass, H.; Bittersmann-Weidlich, E.; Andreasson, L.-E.; Bonigk, B.; Lubitz, W. *Chem. Phys.* **1995**, *194*, 419−432.
(16) Kass, H.; Fromme, P.; Witt, H.; Lubitz, W. *Biophys. J.* **1994**, *66*, A228.
(17) Davis, I. H.; Heathcote, P.; MacLachlan, D. J.; Evans, M. C. W. *Biochim. Biophys. Acta* **1993**, *1143*, 183−189.
(18) Kass, H.; Fromme, P.; Lubitz, W. *Chem. Phys. Lett.* **1996**, *257*, 197−206.
(19) Kass, H.; Lubitz, W. *Chem. Phys. Lett.* **1996**, *251*, 193−203.
(20) Kass, H.; Rautter, J.; Bonigk, B.; Hofer, P.; Lubitz, W. *J. Phys. Chem.* **1995**, 436.
(21) Lendzian, F.; Huber, M.; Isaacson, R. A.; Endeward, B.; Plato, M.; Bonigk, B.; Mobius, K.; Lubitz, W.; Feher, G. *Biochim. Biophys. Acta* **1993**, *1183*, 139−160.
(22) Mac, M.; Tang, X.-S.; Diner, B. A.; McCracken, J.; Babcock, G. T. *Biochemistry* **1996**, *35*, 12388−13293.
(23) Rippke, R.; DeRuelles, J.; Waterbury, J. B.; Herdman, M.; Starkier, R. Y. *J. Gen. Microbiol.* **1979**, *111*, 1−61.
(24) Noren, G. H.; Boerner, R. J.; Barry, B. A. *Biochemistry* **1991**, *30*, 3943.
(25) Bender, C. J.; Sahlin, M.; Babcock, G. T.; Barry, B. A.; Chandrashekar, T. K.; Salowe, S. P.; Stubbe, J.; Lindstron, B.; Petersson, L.; Ehrenberg, A.; Sjoberg, B.-M. *J. Am. Chem. Soc.* **1989**, *111*, 8076−8083.
(26) Kevan, L.; Kispert, L. D. *Electron Spin Double Resonance Spectroscopy*; John Wiley & Sons: New York, 1976.

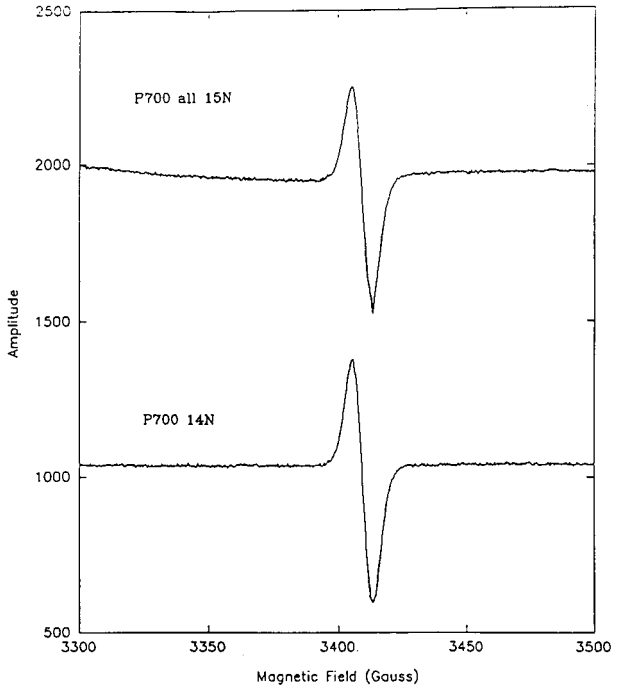

Figure 1. EPR spectra of P_{700}^+ containing natural abundance (top) and isotopically enriched with ^{15}N (bottom). Spectrometer conditions: microwave power, 20 dB; center field, 338.0 mT; modulation amplitude, 0.0125 mT_{pp}; modulation frequency, 100 kHz; time constant, 200 ms; sweep time, 200 s; sample temperature, 8 K.

where $\nu_n = A_{iso}/2$. However, in frozen solution, the anisotropy of the hyperfine coupling gives rise to powder line shapes described to first order by

$$\nu_+ = \nu_n \pm A/2$$

where $A = A_{||} \cos^2 \theta + A_\perp \sin^2 \theta$.

$A_{||}$ and $A_\perp$ in the above expression are the principal values of the axially symmetric hyperfine tensor, and θ describes the orientation of the principal axis system of the hyperfine tensor with respect to the laboratory magnetic field.[27]

ESEEM Data Collection and Analysis. ESEEM data were collected on a home-built spectrometer[28] by using a reflection cavity with either folded stripline[29] or $3\lambda/4$ slotted-tube[30] structures serving as the resonant element. A three pulse or stimulated echo ($90°-\tau-90°-T-90°$) pulse sequence was used. Dead time reconstruction was performed prior to Fourier transformation as described.[31] Computer simulations of the ESEEM data were performed on a Sun Sparcstation 2 computer utilizing FORTRAN software based on the density matrix formalism of Mims.[32] The analysis software for the treatment of experimental and simulated ESEEM data was written with Matlab (Mathworks, Nantick, MA). The experimental dead time was included in the simulations. An isotropic *g*-tensor was assumed in all of the calculations. The success of the spectral simulations was based on the modulation depth and duration observed in the time domain traces as well as the line shapes, peak positions, and relative peak intensities in the frequency spectra.

Results

The continuous wave EPR spectra from P_{700}^+ containing natural abundance ^{14}N (bottom) and isotopically enriched with ^{15}N (top) are shown in Figure 1. The spectra consist of a single peak centered at $g = 2.0025$ with a line width of 0.7−0.75 mT and no observable fine structure. ESEEM spectroscopy was used to resolve the small hyperfine couplings not observed in this inhomogeneously broadened line. The data were collected at magnetic field positions corresponding to the zero-field crossing in the EPR spectrum.

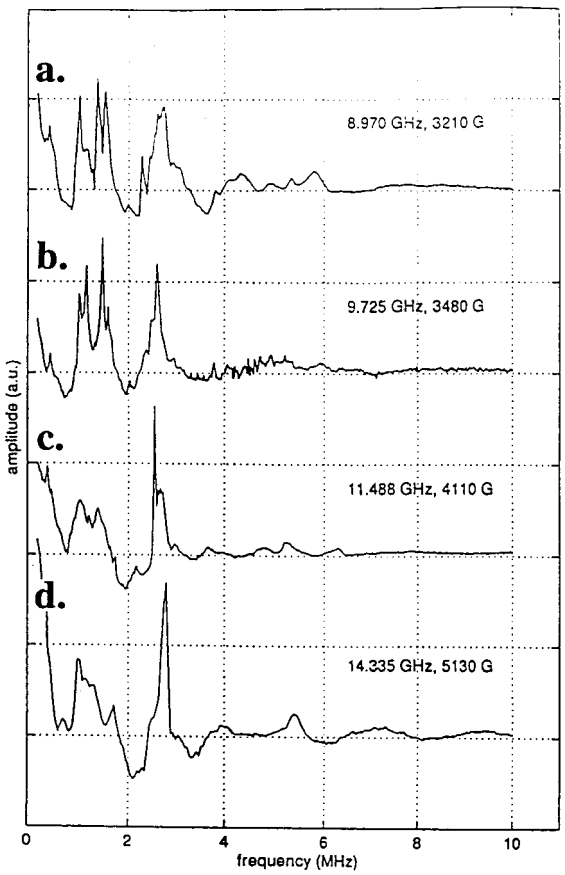

Figure 2. Cosine Fourier transformations of three-pulse ESEEM time domain traces at multiple microwave frequencies from P_{700}^+ containing natural abundance ^{14}N. Spectrometer conditions: magnetic field strength, as noted; τ value, (a) 250 ns, (b) 162 ns, (c) 300 ns, (d) 400 ns; microwave pulse power, (a) 45 dBm, (b) 49 dBm, (c) 55 dBm, (d) 60 dBm; pulse repetition rate, (a) 20 Hz, (b) 60 Hz, (c) 30 Hz, (d) 60 Hz; pulse width (fwhm), 22 ns; sample temperature, 4.2 K.

Cosine Fourier transformation of time domain ESEEM data from stimulated echo experiments collected at multiple microwave frequencies of P_{700}^+ containing natural abundanace ^{14}N are shown in Figure 2 a−d. These spectra are dominated by the nuclear quadrupole coupling of the ^{14}N nuclei in the chlorophyll macrocycle. If the hyperfine interaction of these nitrogen nuclei is approximately equal to twice their nuclear Zeeman frequency, then the energy level splittings in the spin manifold where these two couplings cancel is determined primarily by the ^{14}N nuclear quadrupole interaction. To determine the magnetic field strength at which this exact cancellation condition is met, ESEEM experiments were performed at multiple microwave frequencies.

The exact cancellation ESEEM pattern is characterized by modulations that are deep and long-lived, while the corresponding Fourier transformed spectrum exhibits three sharp, low-frequency features (two of which add up to the third); these

(27) Blinder, S. M. *J. Chem. Phys.* **1960**, *33*, 748−752.
(28) McCracken, J.; Shin, D.-H.; Dye, J. L. *Appl. Magn. Reson.* **1992**, *3*, 30.
(29) Lin, C. P.; Bowman, M. K.; Norris, J. R. *J. Magn. Res.* **1985**, *65*, 369−374.
(30) Mehring, M.; Freysoldt, F. *J. Phys. E: Sci. Instrum.* **1980**, *13*, 894−895.
(31) Mims, W. B. *J. Magn. Reson.* **1984**, *59*, 291−306.
(32) Mims, W. B. *Phys. Rev. B* **1972**, *5*, 2409−2419.
(33) Flanagan, H. L.; Singel, D. J. *J. Chem. Phys.* **1987**, *87*, 5606−5616.
(34) Mims, W. B.; Peisach, J. *J. Chem. Phys.* **1978**, *69*, 4921−4930.

correspond to the zero-field nuclear quadrupole transitions (ν_+ and ν_0) and may be calculated directly from the experimental ESEEM spectrum by using[33,34]

$$\nu_+ = (^3/_4)e^2qQ(1 \pm \eta/3)$$

$$\nu_0 = (^1/_2)e^2qQ\eta$$

where e^2qQ, the quadrupole coupling constant, and η, the asymmetry parameter, describe the magnitude and the symmetry of the electric field gradient tensor. Also characteristic of exact cancellation is a broad $\Delta M_I = 2$ or "double quantum" transition arising from the spin manifold in which the nuclear Zeeman and hyperfine coupling are additive. This transition is observed at approximately four times the nuclear Zeeman frequency and features a line shape that depends strongly on the anisotropy of the hyperfine coupling and the relative orientation of the NQI and hyperfine tensors.

Figure 2b shows qualitatively that this exact cancellation condition is realized for at least two sets of nitrogen nuclei at a magnetic field strength of 348.0 mT. This spectrum contains five major low-frequency components at 1.04, 1.15, 1.47, 1.60, and 2.60 MHz. From the positions of these peaks and by using the equations above, the nuclear quadrupole parameters can be determined for two sets of nitrogens: set A, $e^2qQ = 2.70$ MHz and $\eta = 0.85$; set B, $e^2qQ = 2.81$ and $\eta = 0.73$.

A striking feature of the ESEEM spectrum shown in Figure 2b is the low resolution and intensity found for the ^{14}N double quantum transitions. Because these features carry most of the information regarding hyperfine interactions, reaction centers uniformly labeled with ^{15}N ($I = {}^1/_2$) were studied. The ^{15}N nucleus has no quadrupole moment, and therefore, the stimulated echo modulation pattern is determined by hyperfine and nuclear Zeeman interactions. The multifrequency stimulated echo ESEEM spectra from P_{700}^+ enriched with ^{15}N are shown in Figure 3. The modulations present in this figure arise from hyperfine coupling between the unpaired π electron and nitrogen nuclei in the chlorophyll macrocycle. These spectra, unfortunately, only exhibit two features: a large, sharp feature at low frequency and a broader feature in the 2−4 MHz region. The lack of resolution in the spectra from the ^{15}N-enriched samples precludes definitive determination of the hyperfine coupling constants and number of nuclei giving rise to the observed peaks.

Assignments of magnetic properites to specific nuclei from the data in Figures 2 and 3 can be achieved, however, by performing spectral simulations of the experimental data. The success of these simulations depends on the validity of both the magnitude of the nitrogen hyperfine and quadrupole coupling constants as well as the number of nuclei giving rise to a particular coupling. To make unambiguous assignments of nitrogen hyperfine coupling constants for P_{700}^+, the nitrogen hyperfine coupling tensors and nuclear quadrupole parameters determined must simulate successfully all of the ESEEM spectra in Figures 2 and 3.

Because the observed modulations may arise from several interacting nitrogen nuclei, with each nitrogen requiring seven independent simulation parameters ($A_{||}$, $A_\perp$, e^2qQ, η and the Euler angles α,β,γ describing the relative orientation of the hyperfine and quadrupolar axes), the determination of a unique set of parameters is severely underdetermined. To assist in the assignment of ESEEM features and provide constraints for the simulations, ENDOR experiments were performed on the ^{15}N-enriched P_{700}^+ sample (Figure 4). Features in the low-frequency (1−5 MHz) region of this spectrum are expected to arise from

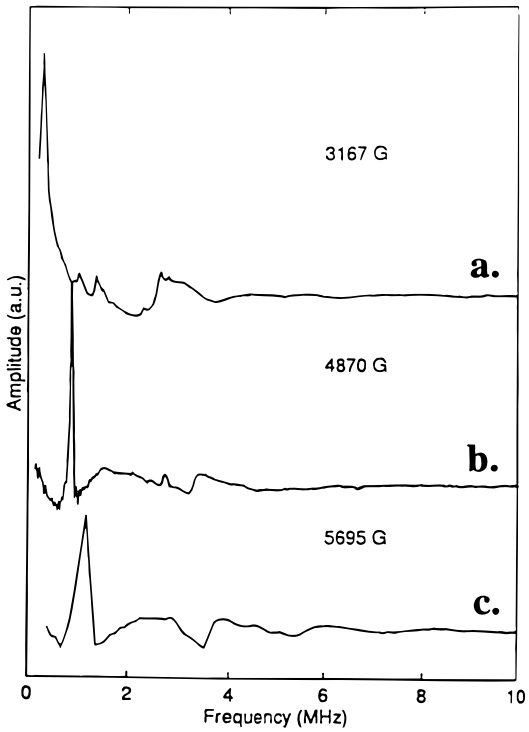

Figure 3. Cosine Fourier transformations of three-pulse ESEEM time domain traces at multiple microwave frequencies from P_{700}^+ isotopically enriched with ^{15}N. Spectrometer conditions: magnetic field strength, as noted; τ value, (a) 222 ns, (b) 318 ns, (c) 400 ns; microwave pulse power, (a) 45 dBm, (b) 45 dBm, (c) 57 dBm; pulse repetition rate, (a) 90 Hz, (b) 30 Hz, (c) 30 Hz; pulse width (fwhm), 22 ns; sample temperature, 4.2 K.

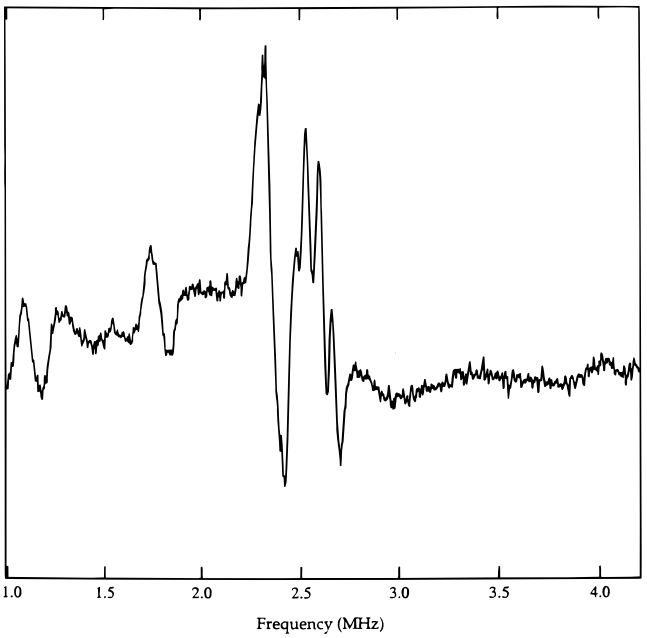

Figure 4. ENDOR spectrum collected at 6 K for P_{700}^+ isotopically enriched with ^{15}N. Spectrometer conditions: microwave power, 1.99 mW; magnetic field strength, 337.5 mT; RF power, 200 W; RF frequency modulation, 100 kHz.

^{15}N nuclei coupled to the π electron in P_{700}^+. Peaks at 1.12 and 1.78 MHz, which are split symmetrically about the nuclear Larmor frequency for ^{15}N (1.46 MHz at 337.5 mT), were previously assigned to the magnetic coupling between P_{700}^+ and an axial histidine ligand.[22]

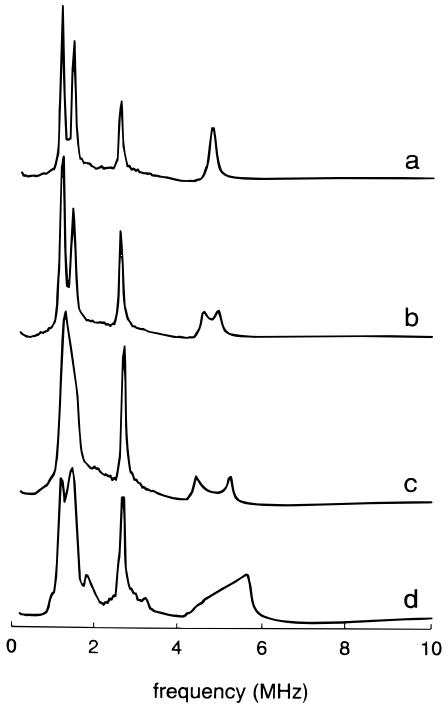

Figure 5. The effect of hyperfine anisotropy on the ESEEM spectrum. Simulation parameters for all spectra, unless otherwise indicated: A 1.84 MHz (a), 1.64 MHz (b), 1.44 MHz (c), 1.44 MHz (d); $A_{||}$ 2.17 MHz (a), 2.56 MHz (b), 2.97 MHz (c), 2.97 (d); A_{iso} 1.95 MHz; e^2qQ 2.69 MHz; η 0.87; magnetic field strength, 348.0 mT; τ value 162 ns; Euler angles (α,β,γ) 0,0,0 and 0,90,0 for d only.

Because the features in the 2−3 MHz region disappear when the sample is specifically labeled with ^{15}N histidine,[22] they are assigned to hyperfine interactions between P_{700}^+ and the pyrrole nitrogens in the chlorophyll macrocycle. These peaks most likely represent the perpendicular components of the hyperfine coupling tensor in one spin manifold. The corresponding transitions from the other manifold, expected to be split symmetrically about ν_n for ^{15}N (1.46 MHz), occur at frequencies less than 1 MHz and, therefore, are not resolved with our spectrometer. It is possible, however, to make some predictions on the strength of the hyperfine coupling based on the peak positions and line shapes. For example, if the derivative shaped feature at 2.35 MHz, can be assigned to the perpendicular singularity of a nitrogen hyperfine tensor, then a corresponding $A_\perp$ value of 1.78 MHz is obtained. Because the number of orientations that contribute to the perpendicular singularity is larger than the number contributing to the parallel component, resolution of the corresponding $A_{||}$ feature is often difficult with ENDOR.

Fortunately, the ESEEM data can be used to provide an estimate of the magnitude of $A_{||}$. At exact cancellation, the hyperfine coupling is equal to twice the nuclear Larmor frequency. Figure 2b shows that this condition is realized at a magnetic field of 348.0 mT, where the nuclear Larmor frequency for ^{14}N is 1.07 MHz. The hyperfine coupling corresponding to this is 2.14 MHz, which, when scaled to the ^{15}N nucleus (^{15}N/^{14}N = 1.403) yields an isotropic coupling of 3.00 MHz. The corresponding peak positions of the $A_{||}$ singularity can be determined. Setting $^1/_3$ ($2A + A_{||}$) = 3.0 MHz yields an approximate $A_{||}$ value of 5.4 MHz and a position for this high-frequency $A_{||}$ turning point in the ^{15}N ENDOR spectrum of $\nu_{15N} + A_{||}/2 = 4.1$ MHz. A small negative feature is observed in this region (Figure 4), which is assigned to the $A_{||}$ turning point of one nitrogen hyperfine coupling. The use of axially symmetric tensors for the tetrapyrrole nitrogens in P_{700}^+ is consistent with those determined experimentally for model chlorophyll and bacteriochlorophyll compounds.[14,35]

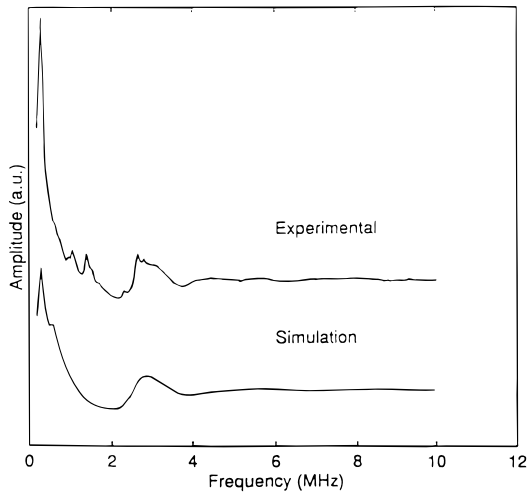

Figure 6. Experimental (top) and simulated (bottom) ESEEM spectra for P_{700}^+ isotopically enriched with ^{15}N. Experimental conditions as in Figure 3A. Simulation parameters as in Table 2.

The improved resolution of this ^{15}N ENDOR spectrum can be used to assist in constraining the parameters needed to perform the numerical simulations of the ESEEM data. Three additional $A_\perp$ features can be measured from the positions of the peaks in the ENDOR spectrum. These couplings, with magnitudes of 2.14, 2.30, and 2.42 MHz, scaled to the appropriate ^{14}N values, and the two sets of quadrupole parameters, determined from Figure 2b, provide a starting point for other simulations.

The lack of features in the double quantum region of the ESEEM spectrum also provides insight into the magnitude of the dipolar contribution to the total nitrogen hyperfine coupling. Briefly, the line shape observed for this modulation component covers a frequency range determined by the extent of hyperfine anisotropy and displays an intensity pattern governed by the relative orientation of NQI and hyperfine tensors.[36] These effects are illustrated in Figure 5. Each calculated ESEEM spectrum in this figure has the same isotropic hyperfine coupling; the dipolar contribution to the total hyperfine coupling in each case, however, is different. Figure 5a−c shows the effects of increasing the hyperfine anisotopy while maintaining the relative tensor orientations at $\alpha,\beta,\gamma = 0,0,0$. As the anisotropy increases the intensity and line widths of the double quantum and low-frequency components are affected. Figure 5d shows an ESEEM simulation obtained by using identical Hamiltonian parameters to those of Figure 5c, except that the principal axes of the hyperfine and NQI tensors are now 90° apart ($\alpha,\beta,\gamma = 0,90,0$ for Figure 5d vs 0,0,0 for Figure 5c). Because the double quantum peaks are missing from the ESEEM spectrum collected at 348.0 mT and our ESEEM data show evidence for at least two sets of narrow "quadrupole" peaks, a considerable amount of anisotropy must be present in the hyperfine coupling of at least two nitrogens.

Further insight into the form of the hyperfine and quadrupole tensors can be gained by examination of the ESEEM spectrum collected at 411.0 mT (Figure 2c). The presence of sharp, intense low-frequency features in this spectrum indicates the exact

(35) Kass, H.; Bittersmann-Weidlich, E.; Andreasson, L.-E.; Bonigk, B.; Lubitz, W. *Chem. Phys.* **1995**, *194*, 419.

(36) Singel, D. J. Multifrequency ESEEM: Perspectives and Applications. In *Advanced EPR*; Hoff, A. J., Ed.; Elsevier: Amsterdam, The Netherlands, 1989; pp 119−134.

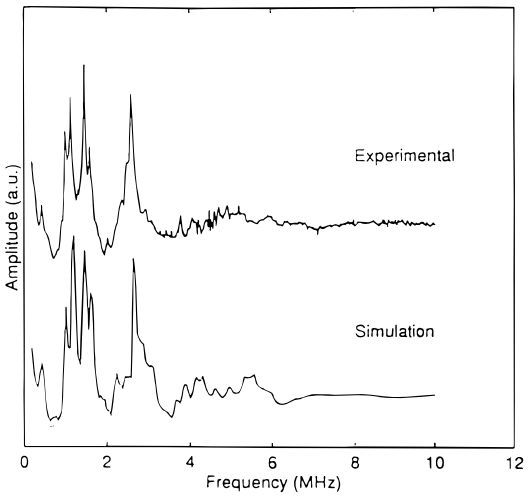

Figure 7. Experimental (top) and simulated (bottom) ESEEM spectra for P_{700}^+ containing natural abundance ^{14}N. Experimental conditions as in Figure 2b. Simulation parameters as in Table 1.

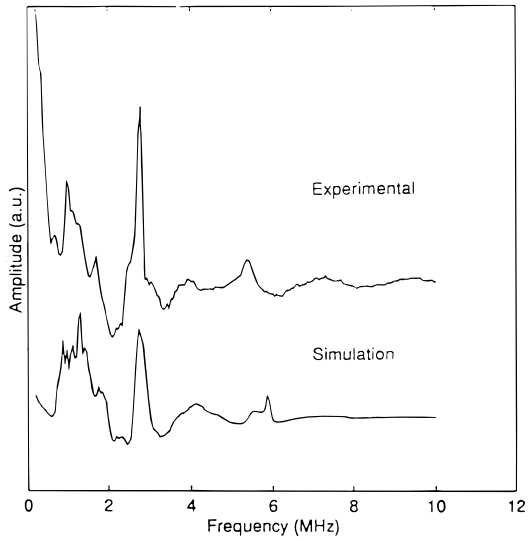

Figure 8. Experimental (top) and simulated (bottom) ESEEM spectra for P_{700}^+ containing natural abundance ^{14}N. Experimental conditions as in Figure 2D. Simulation parameters as in Table 1.

cancellation condition is satisfied for an additional set of nitrogen nuclei. The depth and duration of the modulations observed in the time domain trace corroborate this observation (data not shown). The presence of two, rather than three, sharp quadrupole features is not consistent with the aforementioned description of the NQI tensors determined from the observations made at lower field strength. These findings at 411.0 mT are best explained by an additional set of ^{14}N couplings characterized by a nearly axial NQI tensor and a slightly greater hyperfine coupling.

Utilizing these experimental constraints together with the four distinct $A_\perp$ values measured from the ^{15}N-ENDOR spectrum, successful numerical simulations of the ESEEM data for both ^{15}N and ^{14}N nuclei at multiple microwave frequencies were possible. Figures 6−8 compare the simulations and experimental data for P_{700}^+ containing natural abundance ^{14}N (at 348.0 mT, Figure 7, and at 513.0 mT, Figure 8) and isotopically enriched with ^{15}N (at 316.7 mT, Figure 6). The parameter sets for these simulations are tabulated (see Tables 1 and 2). Excellent agreement between these simulations and the experimental spectra was found at the lower field strength (Figures 6 and 7). The comparison between experiment and theory at Ku-band (Figure 8) is satisfactory in that the changes in the predicted

Table 1. ^{14}N ESEEM Simulation Parameters

	$A_\perp$ (MHz)	$A_{\|\|}$ (MHz)	A_{iso} (MHz)	e^2qQ (MHz)	η	α	β	γ
N_I	1.55	3.29	2.13	2.69	0.87	0	90	0
N_{II}	1.27	3.66	2.06	3.10	0.20	0	0	0
N_{III}	1.64	2.56	1.95	2.69	0.87	0	90	0
N_{IV}	1.73	3.10	2.19	2.81	0.70	0	0	0

Table 2. ^{15}N ESEEM Simulation Parameters

	$A_\perp$ (MHz)	$A_{\|\|}$ (MHz)	A_{iso} (MHz)	r (Å)
N_I	2.17	4.62	2.99	2.13
N_{II}	1.78	5.13	2.89	1.93
N_{III}	2.30	2.67	2.73	2.65
N_{IV}	2.43	4.35	3.07	2.32

ESEEM frequency, amplitude, and line widths that occur as a consequence of increasing the magnetic field from 348.0 to 513.0 mT follow the same trends as those observed experimentally. The sharp feature near 6 MHz in the simulation of these data is not resolved experimentally and is most likely a consequence of the assumption of axial symmetry for all four nitrogen hyperfine tensors in our modeling.

The peaks in the experimental spectrum from ^{15}N-enriched P_{700}^+ that are not reproduced in the simulation are the result of residual ^{14}N contamination. Mass spectrometry of the ^{15}N-enriched P_{700}^+ sample confirms the presence of this ^{14}N (data not shown). Because the ESEEM originating from the ^{14}N nuclei near exact cancellation interactions is so strong, even residual amounts of this nucleus can be observed in the ESEEM spectrum, and moreover, the positions of these features in the ^{15}N spectrum correspond to the observed frequencies of the peaks in the ^{14}N spectrum (Figure 3b). In the absence of the mass spectroscopy data, these features, which appear in the same low-frequency region of the spectrum as those arising from ^{15}N, may have been erroneously assigned to ^{15}N resonances.

Discussion

The availabilty of single crystals of PSI has resulted in much progress toward the elucidation of an electronic structure for P_{700}^+. Single crystal and powder ESEEM studies of PSI containing either ^{14}N or ^{15}N by Lubitz and co-workers have clearly established that the unpaired spin in P_{700}^+ is delocalized asymmetrically.[15,16,19] Furthermore, ESEEM studies by Kass and Lubitz[18] as well as by Davis et al.[17] have yielded many of the nuclear quadrupole coupling parameters. Although significant progress has been made[17,37,38] in the determination of the electronic structure of P_{700}^+, there remains some ambiguity in both the magnitudes of the magnetic coupling parameters and the degree of asymmetry in the delocalization of the unpaired electron. By using a combination of istopic labeling, multifrequency ESEEM, ENDOR, and numerical simulations of experimental ESEEM data, we have been able to identify these parameters for the nitrogen nuclei in P_{700}^+.

Analysis of the peaks observed in the ESEEM spectrum can be difficult as the number of combination peaks arising from multiple nuclei precludes the definitive assignment of these features. The coupling from the axial histidine ligand to P_{700}^+, however, has been shown not to contribute to the ESEEM modulation pattern[22] and therefore eliminates these moieties as

(37) Dikanov, S. A.; Astashkin, A. V.; Tsvetkov, Y. D.; Goldfeld, M. G. *Chem. Phys. Lett.* **1983**, *101*, 206−210.
(38) Astashkin, A. V.; Dikanov, S. A.; Tsvetkov, Y. D. *Chem. Phys. Lett.* **1988**, *152*, 258−264.

possible contributors to the line shape. The similar magnetic properties of the remaining nitrogen nuclei result in the presence of multiple combination lines in the ESEEM spectrum. Moreover, these peaks are clustered together in the 1−5 MHz region of the spectrum and definitive assignment of peaks to specific nitrogen nuclei is impossible without reliable spectral simulations.

Numerical simulations of experimental ESEEM data can be misleading as well since the number of independent parameters required for a system like P_{700}^+, which contains multiple quadrupolar nuclei, severely underdetermines the calculation. To constrain the calculation, information regarding the magnitude of these parameters can be obtained from model compound studies, from studies of other naturally occurring chlorin radicals, or from theoretical calculations modeling the species in vivo and in vitro. Constraints can also be provided by experimental results from other spectroscopic methods or by using isotopic substitution to eliminate specific contributions.

A combination of these methods has been used to constrain the parameter sets in this study. Perhaps one of the most useful of these constraints was the ability to obtain results from ESEEM experiments performed at multiple microwave frequencies. Because the electron−nuclear interaction depends, in part, on the nuclear Zeeman effect, modulation frequencies are dependent on the external magnetic field strength. More importantly, the quantum mechanical mixing of the nuclear states is also varied as the strength of the nuclear Zeeman interaction is changed, and this can result in pronounced changes in ESEEM spectral amplitudes. For this study, multiple frequency ESEEM allowed the exact cancellation condition for coupled ^{14}N nuclei to be enhanced selectively. In the case of P_{700}^+, the ability to perform multiple frequency experiments proved to be especially advantageous because all of the ^{14}N couplings were close to the exact cancellation condition. The discovery of an additional set of quadrupole parameters at 11 GHz that was not observed at the lower microwave frequecies demonstrates how sensitive ESEEM is to small deviations from this resonance condition.[36]

The quadrupole coupling constants and asymmetry parameters for the pyrrole nitrogens in P_{700}^+ listed in Table 1 are consistent with those determined for chlorophyll and bacteriochlorophyll species studied in vivo and in vitro.[17,37,39,40] Because η can be affected dramatically by small changes in orbital occupancies,[41] local electron density distribution differences that give rise to the slight discrepancies for three of the pyrrole nitrogens compared to those of chl a^+ are, most likely, due to interactions with the protein. The asymmetry parameter for N_{II} (see Table 1) is consistent with the value obtained for chl a^+, indicating that the environment of this nitrogen differs somewhat from the other three.[17,18]

The asymmetry parameter is also sensitive to minor changes in the electric field gradient at the ^{14}N nucleus and has been found to shift dramatically as the result of hydrogen bonding and other electrostatic interactions.[41,42] Interactions with charged amino acids or even with the carbonyl or ester functionalities of the other half of the chlorophyll dimer near N_{II} may be responsible for the smaller η values determined for this nucleus. The distance between the two chlorin planes in P_{700} has been determined by X-ray crystallographic studies to be 3.8 ± 0.5 Å, close enough to affect the electric field gradient near the nitrogens.[8,10]

The model of Townes and Dailey, which assumes that the electric field gradient at the nucleus is due only to electrons in the valence 2p orbitals, is a convenient approach for the interpretation of the quadrupole parameters.[43] The axis system in this model assumes that the *z* axis lies along the largest component of the electric field gradient tensor. In a pyrrole compound, the molecular symmetry ensures that one axis of the field gradient tensor lies along the NH bond, one is perpendicular to the molecular plane and the third lies in the molecular plane, perpendicular to the other two.[44] The principal axis is almost always perpendicular to the molecular plane since the p_π orbital contains the lone pair of electrons. In contrast, the *z* axis for the imino nitrogen of imidazole has been found to lie in the plane and is only 4° off of the geometric *z* axis, defined as the bisector of the C−N−C angle.[45] This behavior is in excellent agreement with the Euler angles that were determined from the numerical simulations we have carried out. These angles relate the orientation of the hyperfine axis with respect to the quadrupole axis. For nitrogens I and III, which lie out of the conjugation pathway and therefore are "imino-like" in character, the hyperfine and quadrupole tensor axes are shifted 90° from one another; the principal axis of the hyperfine tensor is perpendicular to the molecular plane, while the principal axis of the quadrupole tensor lies in the plane. This situation is reversed for nitrogens II and IV. Here, the two axis systems are collinear, reflecting the presence of the "pyrrole-like" nitrogens that lie in the conjugation pathway.

A large body of work, both experimental and theoretical, has been aimed at determining the magnitude of the hyperfine couplings for the pyrrole nitrogens in chlorophyll compounds in vivo and in vitro.[15,17,19,37,38] Much of the early spectroscopic work was influenced by single-crystal magnetic resonance experiments performed on the bacterial reaction center.[21,39] The asymmetric spin density distribution motif observed in the bacterial system has been proposed for the primary donor in PSI.[18,19]

Recent spectroscopic investigations of ^{15}N-enriched P_{700}^+ by Kass and Lubitz have been interpreted to indicate that the unpaired electron is 90% delocalized on a single chlorophyll a macrocycle; the other 10% of the spin is distributed over the other half of the geometric dimer.[15,19] This conclusion is based on the observation of small features in the ESEEM spectrum of ^{15}N-labeled P_{700}^+ that previously were not detected. These features correspond to a hyperfine coupling of 0.37 MHz and have been assigned to the nitrogens on the other (10% spin) dimer half. Subsequent ENDOR and HYSCORE experiments by the same laboratory indicated the presence of couplings of this magnitude.[18,19] However, the presence of residual ^{14}N in these ^{15}N-enriched samples, which has been shown to contribute to the ESEEM spectrum even at small concentrations, was not ruled out. The observed peaks, therefore, may result from ^{14}N contamination and not correspond to a hyperfine coupling to the ^{15}N pyrrole nitrogens on the other half of the dimer.

Single-crystal ESEEM studies by Kass et al.[18] also detected five sets of quadrupole couplings in P_{700}^+ that seem to corroborate these results. As with powder samples, single-crystal ESEEM studies are complicated by the presence of multiple combination peaks, however, and unless couplings are confirmed

(39) Lendzian, F.; Lubitz, W.; Scheer, H.; Hoff, A. J.; Plato, M.; Trankle, E.; Mobius, K. *Chem. Phys. Lett.* **1988**, *148*, 377.
(40) Hoff, A. J.; DeGroot, A.; Dikanov, S. A.; Astashkin, A. V.; Tsvetkov, Y. D. *Chem. Phys. Lett.* **1985**, *118*, 40.
(41) Ashby, C. I. H.; Cheng, C. P.; Brown, T. L. *J. Am. Chem. Soc.* **1978**, *100*, 6057.
(42) Jiang, F.; McCracken, J.; Peisach, J. *J. Am. Chem. Soc.* **1990**, *112*, 9035−9044.
(43) Townes, C. H.; Dailey, B. P. *J. Chem. Phys.* **1949**, *17*, 782.
(44) Luckens, E. A. C. *Nuclear Quadrupole Coupling Constants*; Academic Press: New York, 1969.
(45) Blackman, G. L.; Brown, R. D.; Burden, F. R.; Elsum, I. R. *J. Mol. Spectrosc.* **1976**, *60*, 63.

by simulations and multiple microwave frequency experiments, they do not provide definitive proof of these parameters.

The hyperfine and quadrupole coupling parameters listed in Tables 1 and 2, however, are the result of a comprehensive study that incorporated samples containing either natural abundance ^{14}N or isotopically enriched with ^{15}N, followed by multifrequency ESEEM and ^{15}N ENDOR. The couplings we extracted from these spectroscopic studies were confirmed by performing numerical simulations of the ESEEM data. Constraints for these calculations were provided by the multiple magnetic resonance experiments performed, and because simulations utilizing the same parameter set reproduced the experimental multifrequency ESEEM data for both isotopes, these data represent the most complete assignments of hyperfine and quadrupole coupling constants to the pyrrole nitrogens in P_{700}^+ to date.

The $A_\perp$ elements of the hyperfine tensors of P_{700}^+ determined from ENDOR and the corresponding values concluded from simulations of the multifrequency three-pulse ESEEM spectra presented here are identical. The $A_{||}$ components of these tensors were not resolved in the ENDOR, but values for these parameters could be determined through numerical simulations of the multifrequency ESEEM spectra under conditions where limiting values could be established. Isotropic hyperfine coupling constants, determined from exact cancellation stimulated echo ESEEM spectra, helped to place these limits. The use of axial tensors to model the hyperfine interaction of these nuclei is warranted since previous magnetic resonance studies of chlorophyll and bacteriochlorophyll model systems have yielded nitrogen hyperfine couplings of axial symmetry.[15,19,46] Furthermore, theoretical molecular orbital calculations with the RHF-INDO/SP (restricted Hartree−Fock, intermediate neglect of differential overlap-spin polarization) method on chl a cation radicals yielded tensors varying only slightly from axial symmetry.[19,35] Corresponding calculations on the radical in vivo have not been presented in the literature.

These hyperfine couplings can be used to quantify the amount of spin density in the p_π orbital of the individual nitrogen nuclei and therefore provide a probe of the electronic structure of the radical. A full characterization of this structure, however, should include spin density calculations for each nucleus in the species. Multiple ^1H ENDOR experiments on frozen solutions of P_{700}^+ have yielded coupling constants for various positions in the heterocycle. On the basis of the magnitude of these couplings and their corresponding spin densities, an electronic structure model for the radical whereby the unpaired electron is delocalized over a single macrocycle was proposed.[47] The decreased proton hyperfine coupling constants and corresponding carbon spin densities observed for P_{700}^+ in vivo relative to those of the chl a monomer model were attributed to differences in the composition of the ground-state orbital for the two systems. For P_{700}^+, a mixture of 25% of the first excited state and 75% of the ground-state orbital was found to give good agreement between the in vivo and in vitro spin densities.

Analogous spin density calculations were performed for the nitrogen nuclei in P_{700}^+. Because the unpaired spin density on the nitrogens in these radicals resides in the p orbital perpendicular to the plane of the three sp^2 hybrids, the spin density is most accurately determined using the anisotropic part of the hyperfine coupling. The amount of unpaired spin in this orbital is given by the ratio of the measured dipolar coupling, $(A_{||} - A_\perp)/3$, with the corresponding value measured for atomic ^{14}N in the gas phase, 47.8 MHz. The spin densities obtained in this manner for the nitrogen nuclei of P_{700}^+ were multiplied by 1.042 to correct for 2p unpaired spin density in the σ orbitals and are listed in Table 3. [48] Also listed in columns three and four of Table 3 are theoretically determined unpaired spin densities for ground state, D_0, chl a monomer, and for an admixed ground state/excited state (D_0/D_1) model as discussed above.

Table 3. Experimental and Calculated Reduction Factors for P_{700}^+

atom	exptl spin density	calcd spin density, D_0	$D_0(0.25)D_1$ (calcd)	RF	
				calcd	exptl
N1	0.010	−0.013	0.0107	1.2	1.3
N2	0.017	−0.005	0.0205	0.2	0.3
N3	0.007	−0.008	0.0062	1.3	1.1
N4	0.013	−0.001	0.0317	0.03	0.07

In the hybrid orbital model, the experimentally determined spin densities were compared to the spin densities calculated for the ground-state molecular orbital for chl a^+.[47] These experimentally determined "reduction factors" were then compared to those of the theoretically derived hybrid orbital. The reduction factors for C1, C2a, C3, C4, C17, C18, and C_α derived experimentally were in excellent agreement with the theoretically predicted factors. A similar approach was taken with the nitrogen spin densities determined from ESEEM and numerical simulations. As exhibited in Table 3, an excellent match between the experimental and theoretical reduction factors was obtained.

The presence of a hybrid orbital also explains the isotropic hyperfine coupling observed for the axial histidine ligand to P_{700}^+.[22,49] Molecular orbital calculations predict that there is no localized unpaired spin density residing on the Mg^{2+} nucleus for an electron in the ground-state a_{1u} molecular orbital.[50] The first excited-state molecular orbital (a_{2u}), however, is expected to have considerable spin density at this site. Mixing 25% of this excited-state orbital with the ground-state orbital provides the spin density necessary to produce an observable hyperfine coupling to the nitrogen moiety of the axial ligand.

The presence of this axial histidine ligand in P_{700}^+ may explain the admixing of the ground- and excited-state orbitals as it has been shown that the energy splitting between these orbitals can vary with axial ligation.[51] In the bacterial reaction centers, the presence of an axial histidine ligand, which has been confirmed by the high-resolution crystal structure,[52,53] is not expected to induce this mixing since the energy separation between the ground- and excited-state orbitals in bacteriochlorin systems has been found to be larger than in chlorin systems.[51]

Localization of the unpaired electron spin to one of the monomers in the P_{700}^+ special pair assists in elucidating both the function and energetics of the primary donor in oxygenic versus bacterial systems. While homologies exist, both in pigment composition and primary protein structure, between these systems, the primary donors in PSI and PSII appear to be much more weakly coupled dimers of chlorophyll than their bacterial counterpart.[2,54,55] This results in a shallower trap for

(46) Astashkin, A. V.; Dikanov, S. A.; Tsvetkov, Y. D.; Goldfeld, M. G. *Chem. Phys. Lett.* **1987**, *134*, 438−443.
(47) O'Malley, P. J.; Babcock, G. T. *Proc. Natl. Acad. Sci. U.S.A.* **1984**, *81*, 1098−1101.
(48) Gordy, W. *Theory and Applications of Electron Spin Resonance*; John Wiley & Sons: New York, 1980; Vol. XV.
(49) Webber, A. N.; Su, H.; Bingham, S. E.; Kass, H.; Krabbens, S. L.; Kuhn, M.; Jordan, R.; Schlodder, E.; Lubitz, W. *Biochemistry* **1996**, *35*, 12857−12863.
(50) Petke, J. D.; Maggiora, G. M.; Shipman, L. L.; Christoffersen, R. E. *Photochem. Photobiol.* **1980**, *31*, 243−257.
(51) Hansen, L. K. *Molecular Orbital Theory of Monomer Pigments*; Hansen, L. K., Ed.; CRC Press: Boca Raton, FL, 1990; p 1211.
(52) Diesenhofer, J.; Epp, O.; Huber, R.; Michel, H. *Nature* **1985**, *318*, 618.
(53) Allen, J. P.; Feher, G.; Yeates, T. O.; Komiya, H.; Rees, D. *Proc. Natl. Acad. Sci. U.S.A.* **1987**, *84*, 5730.
(54) Golbeck, J. *Proc. Natl. Acad. Sci. U.S.A.* **1993**, 1642−1646.

excitation energy in the higher plant reaction centers. Clearly, an evolutionary correlation between the energetics of charge separation and the ability of plants to oxidize water exists, and a clearer view of the electronic structure of P_{700}^+ is integral in determining this relationship.

Weak coupling, both within the chlorophyll dimer that acts as the primary electron donor and between subsequent electron-transfer cofactors, may help to explain the observed thermodynamic differences. In the bacterial system, the shift in optical absorption of the species in vivo versus in vitro is large, also indicative of strong intradimer coupling.[51] The unpaired spin is delocalized in a 2:1 ratio over the two halves of the bacteriochlorophyll a (bchl a) dimer,[21] consistent with the increased excitonic coupling apparent in the reaction center special pair optical spectrum. Conversely, for P_{700}^+, the weak coupling between dimer halves prevents delocalization of the unpaired electron spin, and the distribution is monomeric. The analogous red shift in optical absorption is smaller for the chlorophyll species. The relationship between the degree of excitonic coupling, which is modulated by the protein environment, and the optical absorption is exhibited most effectively by the light harvesting complexes from the bacteria *Rb. acidophila*, for which a high-resolution crystal structure is available.[56] In these complexes, two of the three bchl a molecules involved in light harvesting absorb light of a considerably longer wavelength than the third (850 vs 800 nm) and are substantially red shifted from the pigment in vitro (773 nm). This pair of pigments (B_{850}) is in close contact in the hydrophobic membrane protein environment, which promotes the strong exciton coupling observed. Similarly, with the bacterial reaction center special pair bacteriochlorophylls, close physical juxtaposition promotes strong exciton coupling that produces the significant absorption red shifts observed in these systems. The magnetic resonance manifestation of this close physical interaction is the delocalization of unpaired spin density over both halves of the dimer.

For P700, the extent of the absorption red shift, relative to both monomeric chlorophyll in vitro and to the antenna pigments in PSI, is significantly less, reflecting the weak coupling that we detect in the magnetic resonance properties. This weaker exciton coupling most likely derives from the slightly increased intradimer distance in the special pair as compared to the bacteria. The perpendicular center-to-center distance in P_{700}^+ has been estimated to be 3.8 ± 0.5 Å[10] versus 3.5 Å[57] in the bacterial reaction centers. This, combined with differences in the protein environment, may explain the observed differences in exciton energetics.

The weaker coupling that is observed in PSI, and also in PSII[2], has significant thermodynamic consequences, as it carries through to the conversion of photon energy into chemical potential. In the bacterial reaction center, only about 0.5 eV of the incident photon energy is conserved in the $P^+Q_A^-$ state. Taking P_{870} in sphaeroides, which absorbs photons of energy 1.43 eV, as a reference, this represents a conversion efficiency of about 35%. In PSI, the free energy difference between P_{700}^+ and the reduced primary acceptor, F_x, is on the order of 1.2 eV.[6−8] Thus, of the 1.8 eV photon that initiates photochemistry in PSI, almost two-thirds of the energy is captured by the plant as chemical potential. A similar situation occurs in PSII, that is, conversion efficiencies approaching two-thirds are observed.[2] The evolutionary development that allowed plants to acquire the ability to use water as the electron donor undoubtedly derives from the greater efficiencies with which their reaction centers convert light energy into useful free energy. Weaker coupling, both in exciton and magnetic interactions and in thermodynamic driving forces, appears to have been the strategy that was successful.

In conclusion, the data reported here represent the most complete assignments of hyperfine and quadrupole coupling constants to the nitrogen nuclei in P_{700}^+ made to date. The magnitude of the hyperfine couplings and their corresponding spin densities are indicative of a monomeric chlorophyll a cation radical interacting with its protein environment through axial ligation or hydrogen bonding. These effects cause an admixing of the ground-state and first excited-state molecular orbitals to create a hybrid orbital with an altered spin density distribution when compared to chlorophyll cation radical species in vitro. Additionally, the methodology utilized to determine these parameters, a combination of isotope enrichment, electron magnetic resonance spectroscopy, and numerical simulations, provides a means by which complicated couplings in biological systems can be consistently and systematically evaluated.

Acknowledgment. This work is supported by the National Institutes of Health Grants GM-54065 (J.M.) and GM-37300 (G.T.B.) and the USDA CRGO Photosynthesis Program (G.T.B.). EPR instrumentation was purchased, in part, with funds supplied by the NIH through grant number RR10381 (J.M. and G.T.B.). Mass spectral data were obtained at the Michigan State University Mass Spectrometry Facility, which is supported, in part, by a grant (DRR-00480) from the Biotechnology Program, National Center for Research Resources, National Institutes of Health.

JA982662I

(55) Durrant, J. R.; Klug, D. R.; Kwa, S. L. S.; VanGrondelle, R.; Porter, G.; Dekker, J. P. *Proc. Nat. Acad. Sci.* **1995**, *92*, 4798−4802.

(56) McDermott, G.; Prince, S. M.; Freer, A. A.; Hawthornthwaite-Lawless, A. M.; Papiz, M. A.; Cogdell, R. G.; Isaacs, N. W. *Nature* **1995**, *374*, 517.

(57) Yeates, T. O.; Komiya, H.; Chirino, A.; Rees, D. C.; Allen, J. P.; Feher, G. *Proc. Natl. Acad. Sci. U.S.A.* **1988**, *85*, 7993−7997.